JGR Atmospheres

RESEARCH ARTICLE
10.1029/2018JD029419

Special Section:
Fog: Atmosphere, biosphere, land, and ocean interactions

Impact of Air Pollution Controls on Radiation Fog Frequency in the Central Valley of California

Ellyn Gray[1], S. Gilardoni[2], Dennis Baldocchi[1], Brian C. McDonald[3,4], Maria Cristina Facchini[2], and Allen H. Goldstein[1,5]

[1]Department of Environmental Science, Policy and Management, Division of Ecosystem Sciences, University of California, Berkeley, CA, USA, [2]Institute of Atmospheric Sciences and Climate - National Research Council (ISAC-CNR), Bologna, BO, Italy, [3]Cooperative Institute for Research in Environmental Science, University of Colorado, Boulder, CO, USA, [4]Chemical Sciences Division, NOAA Earth System Research Laboratory, Boulder, CO, USA, [5]Department of Civil and Environmental Engineering, University of California, Berkeley, CA, USA

Key Points:
- Central Valley fog frequency increased 85% from 1930 to 1970, then declined 76% in the last 36 winters, with large short-term variability
- Short-term fog variability is dominantly driven by climate fluctuations
- Long-term temporal and spatial trends in fog are dominantly driven by changes in air pollution

Supporting Information:
- Supporting Information S1
- Table S1
- Table S2
- Figure S1
- Figure S2
- Figure S3
- Figure S4
- Figure S5

Correspondence to:
E. Gray,
ellyngray@berkeley.edu

Citation:
Gray, E., Gilardoni, S., Baldocchi, D., McDonald, B. C., Facchini, M. C., & Goldstein, A. H. (2019). Impact of air pollution controls on radiation fog frequency in the Central Valley of California. *Journal of Geophysical Research: Atmospheres*, *124*. https://doi.org/10.1029/2018JD029419

Received 31 JUL 2018
Accepted 11 MAR 2019
Accepted article online 28 MAR 2019

Abstract In California's Central Valley, tule fog frequency increased 85% from 1930 to 1970, then declined 76% in the last 36 winters. Throughout these changes, fog frequency exhibited a consistent north-south trend, with maxima in southern latitudes. We analyzed seven decades of meteorological data and five decades of air pollution data to determine the most likely drivers changing fog, including temperature, dew point depression, precipitation, wind speed, and NO_x (oxides of nitrogen) concentration. Climate variables, most critically dew point depression, strongly influence the short-term (annual) variability in fog frequency; however, the frequency of optimal conditions for fog formation show no observable trend from 1980 to 2016. NO_x concentration, which has a decreasing north-south concentration gradient, declined continuously over this period, consistent with the long-term temporal and spatial trends in fog. As development in the Central Valley increased direct particle and other pollutant emissions from 1930 to 1970, fog frequency increased. Following the Clean Air Act, particle emissions quickly declined, and NO_x emissions declined steadily, reducing the cloud condensation nuclei (CCN) available for fog formation. As a precursor of ammonium nitrate aerosols, which are efficient CCN, we used NO_x measurements and emission trends as a proxy for the CCN trend. We conclude that while the short-term fog variability is dominantly driven by climate fluctuations, the longer-term temporal and spatial changes in fog have been driven by changes in air pollution. For conditions close to the dew point, a decrease in fog of 5 days/year per 10 parts per billion NO_x decrease occurred across the Central Valley.

Plain Language Summary California's Central Valley is known for dense wintertime ground fog, called tule fog, which dramatically reduces visibility, causing weather-related accidents, while also helping provide the "winter chill" required to improve productivity of fruit and nut trees. Fog frequency changed dramatically over the past century, increasing 85% from 1930 to 1970 then decreasing by ~75% since 1980. We found that climate variables, most importantly dew point depression (a measure of how low the temperature must drop for water droplets to form) is the main controller of short-term (year-to-year) changes in fog frequency. However, changing air pollution is the main driver of the long-term trends in fog frequency because it provides water-attracting particles on which fog droplets form. Air pollution increased in the Central Valley of California prior to 1970 due to development with lack of emissions regulation, then decreased since 1980 due to effective air pollution control, matching the observed long-term trend in fog frequency.

1. Introduction

Understanding the drivers of dense radiation fog, known as tule fog, in California's Central Valley is important for the safety, economic development, and agricultural viability of the region. Central Valley fog events are the primary cause of California's weather-related accidents, making this region a national leader in vision-impaired vehicle collisions (Ashley et al., 2015). Radiation fog also inflicts an economic toll due to delayed aviation and temporary closure of businesses and schools. Thus, a regional decrease in fog events has considerable safety and economic advantages for the valley's 6.5 million residents.

However, the rapid agricultural development in the valley throughout the twentieth-century relied on the increased occurrence of wintertime radiation fog. Prolonged periods of dense fog were ideal for meeting

the required cold season dormancy period of fruit and nut trees, known as "winter chill," to avoid poor fruit set (Baldocchi & Wong, 2008; Luedeling et al., 2009). The region experienced up to 400 fewer hours of winter chill per year in 2012 when compared to 1982 due to a reduction in dense fog (Baldocchi & Waller, 2014). Fog also influences surface conditions by nearly eliminating the vapor pressure deficit that drives evapotranspiration; hence, declining fog can enhance evaporation in an already drought stressed region (Fischer et al., 2009; Williams et al., 2018). As such, understanding the drivers of the tule fog trend holds agricultural value for the valley, which exceeded $40 billion in revenue in 2017 (CFDA, 2018).

Throughout the twentieth-century, trends in tule fog frequency have changed dramatically. While fog frequency increased steadily from 1930 to 1970, with cities such as Fresno seeing an 85% increase in dense fog episodes, analysis from both ground and remote sensing measurements found a 46–50% reduction in fog beginning in 1980 (Baldocchi & Waller, 2014; Herckes et al., 2015). Despite significant research on the thermodynamic contributors to tule fog (Bergot & Guedalia, 1994; Roach et al., 1976), no explanation consistent with the upward-then-downward trend in its frequency over the last century has been identified. This study seeks to elucidate both the long-term contributors to fog enhancement and decline, as well as understand key drivers of short-term variability.

There are a number of anthropogenic meteorology changes that could inhibit maximum radiative cooling, making it more difficult to reach dew point. Notable changes include rising temperatures associated with climate change and/or the urban heat island effect. However, temperature alone as the dominant variable driving the tule fog trend cannot explain the observations, as the rising temperatures associated with both climate change and urban expansion would be largely positive over the past century, unlike the upward-then-downward signal seen in fog frequency. The role of urbanization has also been investigated due to the occurrence of urban clear islands in highly populated Central Valley cities (Lee, 1987; Suckling & Mitchell, 1988), such as in Fresno where dense fog episodes detected via satellite imagery begin dissipating from the center of the urban footprint (Underwood & Hansen, 2008). However, fog decline is apparent in both urban and rural locations when investigated from satellite imagery (Baldocchi & Waller, 2014), suggesting a common driver throughout the valley, rather than just the urban sites. Changes in water availability due to agricultural expansion can also have notable climate effects; however, wintertime irrigation is uncommon during California's rainy season, making it a less likely driver (Salas et al., 2006).

The upward-then-downward trend may be better correlated with Central Valley air pollution trends. The number concentration and composition of aerosols can play a significant role in fog's frequency, density, and persistence, with fog being more likely to occur in regions with high aerosol concentration and low supersaturation (Gultepe et al., 2007). Increased air pollution has been identified as a catalyst for enhanced radiation fog in the past, such as during the deadly London Smog of 1952 (Wilkins, 1954). Subsequent reductions in dense fog episodes in London have been attributed to regulation of emissions through the Clean Air Act of 1956 (Brimblecombe, 1977). Hence, our interest in air pollution as a driver of fog frequency is rooted in observed outcomes of past regulation.

The Central Valley is consistently out of compliance with standards for particulate matter, with air quality assessments ranking it among the worst areas in the nation (American Lung Association, 2016). During the cool, winter months, conditions are ideal for formation of ammonium nitrate (NH_4NO_3), which is the dominant (30–80%) inorganic particulate matter with aerodynamic diameter 2.5 micrometers or less ($PM_{2.5}$); the remaining PM is dominated by organic species (Chow et al., 2006; Pusede et al., 2016). While NH_4NO_3 is a product of ammonia (NH_3) and nitric acid (HNO_3), the high abundance of primary NH_3 from agricultural sources make Central Valley NH_4NO_3 formation HNO_3-limited (Battye et al., 2003; Schiferl et al., 2014). HNO_3 is formed from oxides of nitrogen ($NO_x = NO + NO_2$) through both daytime oxidation by the hydroxyl radical and nighttime oxidation by ozone. Central Valley NH_4NO_3 production is thus very sensitive to changes in NO_x concentration, with reductions in NO_x resulting in corresponding reductions in NH_4NO_3 in $PM_{2.5}$ (Pusede et al., 2016).

NH_4NO_3 is very hygroscopic, making it an ideal cloud condensation nuclei (CCN) for cloud and fog formation at low supersaturation (Petters & Kreidenweis, 2007). Scavenging measurements indicate that ammonium nitrate is effectively removed by fog for nucleation scavenging, confirming its ability to act as CCN at low supersaturation typical of fog (Gilardoni et al., 2014). Additionally, HNO_3 and NH_3, the precursors

to NH_4NO_3 formation, reduce vapor pressure, increasing hygroscopicity and allowing activation at smaller sizes (Kulmala et al., 1998; Andreae & Rosenfeld, 2008). Polluted fog consists of a higher number concentration of small droplets, which in turn increases cloudiness and prolongs the lifetime of clouds and fog (Kulmala et al., 1995). Klemm and Lin (2016) modeled fog formation in regimes with relative humidity (RH) < 100% finding equivalent reductions in fog with increases in temperature and reductions in aerosol concentration, likely tied to changes in hygroscopic gases such as SO_2 and NO_x.

Further, the presence of HNO_3 and NH_3 in water droplets can also alter the hygroscopicity and size of unactivated droplets—droplets that do not reach the supersaturated conditions critical for growth—but can nonetheless yield the impression of dense fog (Charlson et al., 2001; Kokkola et al., 2002; Kulmala et al., 1997; Laaksonen et al., 1998). The hygroscopicity of the NH_3 and HNO_3 allow cloud-droplet-sized particles to form in RH of less than 100%, causing low-visibility, fog-like conditions.

As the primary precursor to ammonium nitrate PM in the Central Valley, we focus on trends in NO_x as an indicator of the impact of changing air pollution on fog frequency.

Here we develop and compare historical records of temporal and spatial patterns for fog events, climatic variables, and air pollution to investigate the dominant drivers for fog frequency and persistence.

2. Study Region

The Sierra Nevada to the east and Coastal Range to the west create ideal valley geography for persistent radiation fog episodes. Tule fog season spans November to March, during which weather conditions are characteristically binary: dry, cloudless days permeated by occasional wet winter storms. Clear conditions favor rapid radiative surface cooling following sunset, and if RH is high and temperature and wind speeds are low, atmospheric moisture can condense to form ground fog. The wintertime inversion causes fog to linger close to the surface, typically below 300 m, constrained horizontally by the perimeter mountain ranges (Bianco et al., 2011; Underwood et al., 2004). The stagnant conditions and low wind speed usually associated with the Great Basin High cause fog events with visibility often below 200 m to persist for as long as 12 to 18 hr, usually dissipating midmorning (Herckes et al., 2015).

The Central Valley has distinct differences in a variety of attributes as a function of latitude including fog occurrence, climate variables, urbanization, and air pollution. For the purposes of analyses in this paper, we divide the study region by latitude and aggregate data for specific representative areas, as shown in Figure 1. To emphasize the spatial gradients of different variables, each degree of descending latitude, beginning at 40°N, is represented by a different color in the spectral color scheme, with cooler colors representing the northernmost locations and warmer colors representing the southernmost.

3. Methods

The longest record of fog frequency available was obtained from the National Oceanic and Atmospheric Administration archive for Fresno dense fog days beginning in 1909. This record wholly encapsulates the upward-then-downward trend in fog frequency observed in the twentieth century that cannot be fully observed in modern records from the National Climatic Data Center (NCDC) which are shorter (1940–2016), but more temporally and spatially complete. However, when compared, both data sets show excellent agreement, thus providing greater confidence for the National Oceanic and Atmospheric Administration data, as analysis will show.

We developed a detailed fog climatology using up to 75 years of visibility measurements from the NCDC spanning 15 sites typically located at airports (https://www7.ncdc.noaa.gov/CDO/cdoselect.cmd). Dense fog was defined as visibility below 400 m (one quarter-mile). The climatology is derived from hourly data wherever possible to account for the highly episodic nature of dense fog. Any day with at least 1 hr of dense fog is considered a fog day, all of which are summed over each fog season (November–March), representing annual fog days per year. In order to calculate annual fog days, each month needed >90% hourly coverage. If all 5 months of the fog season had >90% (with most years included having >98% coverage), annual fog days were summarized. Average duration was determined by dividing the total number of dense fog hours in a winter season by the total fog days.

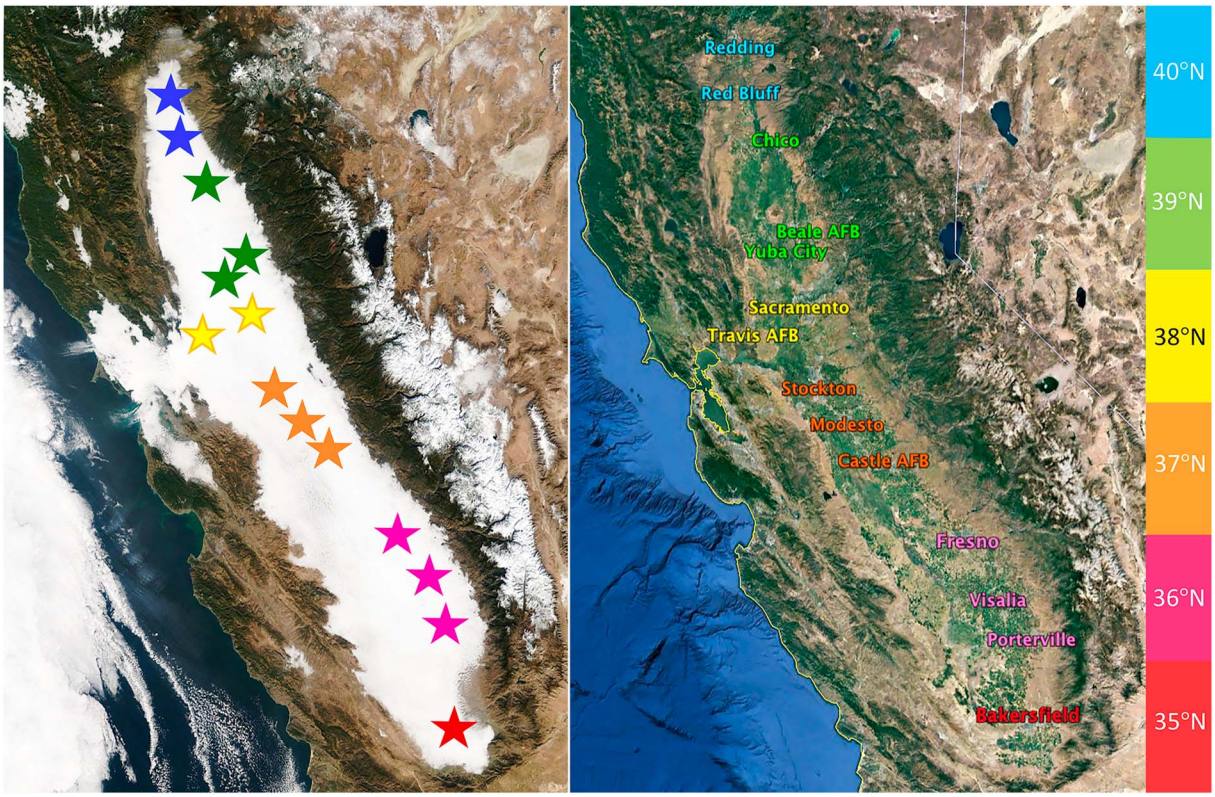

Figure 1. Map of Central Valley sites color coded by latitude from Terra MODIS. Color coding represents change in 1° of latitude, beginning at 40°N. Sacramento contains two sites: Sacramento Executive Airport and Mather Field Airport in Rancho Cordova.

Prior to 1996, visibility was measured by station meteorologists using visible markers, as described in the Surface Aviation Observing guidelines. Modern visibility is instead automatically observed using a forward scatter visibility sensor that measures the attenuation of light at 20-s intervals, with a maximum recorded visibility of 16 km. All visibility observations are thus limited to 16 km for consistency.

Historical records of temperature, dew point, and wind speed from airports throughout the valley were accessed through the NCDC. Daily averages were calculated by extracting measurements taken every 3 hr (eight measurements per day), requiring seven of eight observations to calculate an average. Data for maximum/minimum temperature and precipitation were pulled from daily measurements calculated by the NCDC at the same airports (https://www.ncdc.noaa.gov/cdo-web/datatools/lcd). We set a 65% minimum reporting threshold for daily values to calculate monthly averages for the November–March fog season. We determined 65% as the necessary threshold through random sampling *t* tests of large iterations and requiring deviation from the mean be less than 5%. Annual wintertime (November–March) averages were calculated by averaging over the season, with all 5 months required per season to ensure comparability year over year. Records were inspected for station location continuity whenever possible and reviewed for instrument malfunction.

Trends in particulate matter (PM_{10}) and NO_x emissions were first obtained through the Environmental Protection Agency (EPA) NO_x Emission Inventory from 1940–1998 (EPA, 2000). More modern trends for NO_x emissions from 1970 to 2017 were obtained from the EPA's website (https://www.epa.gov/air-emissions-inventories/air-pollutant-emissions-trends-data). A localized fuel-based emission inventory of NO_x for the San Joaquin Valley and the Central Valley (San Joaquin + Sacramento Valley) was developed using the methods described in McDonald et al. (2012). Briefly, mobile source emissions are estimated using a fuel-based approach, including on-road engines (e.g., passenger vehicles, heavy-duty trucks), off-road diesel engines (e.g., tractors, construction equipment), and small two- and four-stroke off-road gasoline engines.

Mobile source engine activity is estimated using state-level fuel sales reports for on-road and off-road engines and allocated to the San Joaquin and Sacramento Valley air basins using California's 2009 Emissions Almanac (CARB, 2009). Long-term trends in mobile source NO_x emission factors have been characterized from the 1960s to the present day by Hassler et al., 2016. All other anthropogenic sources of emissions are from California's Emissions Almanac, which reports emissions from 1975 to the present day for stationary and area sources. Prior to 1975, we extrapolate stationary and area sources to 1960 based on annual fuel activity data from the State Energy Database System (Energy Information Administration, 2017).

NO_x concentration data were obtained from the California Air Resources Board archive (https://www.arb.ca.gov/adam/). Each city has multiple monitoring stations where NO_x is measured by chemiluminescence and averaged over 24 hr. The length of data recorded at each monitoring station can vary significantly, ranging from a few years to multiple decades. In order to develop a historical record with a similar latitude distribution as the meteorological variables, we selected stations within the urban plume of the local airport meteorological stations, with the largest perimeter being those of Fresno and Bakersfield (14.5 × 13 km). We compared the monitoring stations within each urban plume to confirm consistency of station reporting. After removing severe station outliers, we calculated monthly averages for November–March, requiring 65% of daily measurements per month. Past studies confirmed the representativeness of Central Valley ground-based measurements using NO_2 retrievals from the Ozone Monitoring Instrument (OMI; Russell et al., 2012). We acknowledge that some NO_x data for this study are averaged for a city plume originating as much as 8–15 km from the visibility measurements, which are typically observed at airports. While NO_x does exhibit distinct urban plumes when observed by Ozone Monitoring Instrument past work characterized Central Valley boundary layer pollution as well mixed within latitude bands, especially during frequent multiday pollution episodes and wintertime stagnation (Pusede & Cohen, 2012). Further, Chow et al. (2006) found San Joaquin Valley wintertime NH_4NO_3 $PM_{2.5}$ much more uniformly distributed outside urban plumes than carbonaceous PM, with the zone of representativeness for monitoring sites being between 10 and 20 km, increasing even further when observations were annually averaged. This suggests that the urban monitoring sites are sufficiently representative for this study.

Trends in predictor variables were analyzed using the nonparametric two-tailed Mann-Kendall trend test and the Theil-Sen estimator (http://www.mathworks.com/matlabcentral/fileexchange/authors/23983) (Burkey, 2006). The Mann-Kendall trend test assesses the null hypothesis (H_0), which assumes there is no trend in the data, against the alternative (H_1) without requiring linearity (Mann, 1945; Kendall, 1955). The Mann-Kendall test outputs $H = 0$ when the null hypothesis passes and $H = 1$ when it fails, meaning that there is a statistically significant trend at the $\propto = 0.01$ significance level. The Theil-Sen estimator is a nonparametric technique for robustly fitting data to a line while minimizing the influence of outliers (Sen, 1968; Theil, 1950). The Sen's slope (Q_i) is determined by finding the median of all the slopes between pairs of points over the designated period:

$$Q_i = \frac{(x_j - x_k)}{(j - k)} \text{ for } i = 1, \ldots n,$$

where x_j and x_k are data at times j and k, and n is the number of data points. The average of these n values for Q_i is Sen's slope. A best fit line is calculated using the slope and y intercept. The Theil-Sen estimator was used to determine the average change in each variable per year over the course of the period of inquiry.

In order to separate the high frequency, shorter-term signal from the long-term trend, we first ran a Lomb-Scargle periodogram on daily averages to identify significant periods in the data, despite its uneven sampling (Lomb, 1976; Scargle, 1982). Dew point depression (DPD), temperature, NO_x concentration, wind speed, precipitation, and visibility (as a continuous variable highly correlated with fog days) were analyzed. The input data were processed by normalizing by its 1-norm and detrending before analyzing the output frequencies of highest spectral significance ($p < 0.01$). The frequencies were compared between variables to identify common periods of variability. These periods were used as windows for a low pass filter, calculated by a moving mean, in order to isolate the long-term trend from the high frequency variability, calculated as the residuals of the moving mean. The decomposed trends for DPD, wind speed, and NO_x were then tested for correlation with daily visibility.

Correlation between annual fog days and predictor variables was found using orthogonal linear regression, in which errors in both the dependent and independent variables were determined for the linear fit (https://www.mathworks.com/matlabcentral/fileexchange/16800-orthogonal-linear-regression). The linear correlation was calculated using the Pearson correlation coefficient and was then squared to find the coefficient of determination, which estimates the fraction of variance in fog days explained by the predictor variable. When analyzing the correlation between fog days and air pollution, meteorology of sufficient time resolution for calculating Sen's slopes was not available for Chico, Yuba City, or Modesto. In these instances, data from adjacent meteorological stations were substituted with reporting from Red Bluff, Beale Air Force Base, and Castle Air Force Base, respectively. Meteorology data at the paired sites were highly correlated, with R^2 ranging from 0.81 to 0.88 (supporting information Table S1). Air pollution data were available for a smaller window of 1980–2014. An exception was made for Chico—where observations concluded in 2008—because it is the northernmost site with available NO_x measurements, making these data of great interest.

Table S2 provides a description of the observational sites, including location, length of high resolution operation, and completeness of record from 1963 to 2016 for meteorology and 1963 to 2014 for NO_x concentration.

4. Results and Discussion

4.1. Radiation Fog Trend

4.1.1. Temporal Variability

The number of dense fog days in Fresno, the longest record available, increased 2% per year on average from 1930 to 1970, demonstrating a statistically significant 85% growth ($p < 0.01$). A distinct decrease in fog days began for all locations around 1980, with sites in the north exhibiting the most rapid decline at 2.5% fewer fog days per year (Table 1). Fog decline is most apparent when the trend is averaged over all sites using the hourly NCDC record, demonstrating a valley-wide decrease in both occurrence and duration of fog (black lines in Figure 2). From 1980 to 2016, fog days have declined on average by 76% ($p < 0.01$), with average fog episode per day declining by 56% from a valley-wide average of 6.2 hr/day to 2.7.

Historically, dense fog episodes were characterized by late night low visibility events—particularly in the foggiest locations such as Fresno (Figure S1c)—when the surface radiatively cools. As the cooler conditions continue to favor condensation throughout the night, denser fog develops into the early morning hours, reaching its peak after 5 am. However, the diurnal pattern of wintertime visibility has gradually transitioned since ~1980, with low visibility events now forming in the early morning (fewer blue colors from 20–24 hr) and dissipating more quickly the following day (Figure S1). The reduction in dense fog events demonstrated in Figure 2 has a substantial impact on conditions later in the day, with average afternoon visibility increasing since 1990 at all locations. The impact is seen most strongly in Red Bluff (Figure S1a) where the fog season has nearly ceased to occur.

4.1.2. Spatial Variability

Central Valley fog frequency exhibits a pronounced north-south gradient, with fog consistently more frequent in southern latitudes than northern over the course of the NCDC record (Figure 3). This pattern is represented throughout the analysis by the spectral color scheme, in which cooler colors represent northern latitudes and warmer colors represent southern latitudes. Sites throughout the 700-km-long region have strong year-to-year variability that is coincident, suggesting that large-scale mechanisms control this variability. A deviation from the observed north-south fog gradient is seen in the southernmost city, Bakersfield, which we will explore further in the meteorological analysis.

We use the spatial gradient, in conjunction with the long-term upward-then-downward temporal trend in Figure 2a, to identify drivers of changing fog formation by their correspondence to the unique spatiotemporal features of the fog record.

4.2. Climate Trends

Here we present available trends of the key climatic drivers likely to be associated with fog formation: minimum temperature, DPD, precipitation, and wind speed. Each variable is considered, when possible, for its relationship to the spatial (distinct north-south gradient) and temporal (upward-then-downward signal),

Journal of Geophysical Research: Atmospheres

10.1029/2018JD029419

Table 1
Trends in Wintertime Meteorology (1980–2016) and NO_x Concentration (1980–2014)

Location	Latitude	Fog days		Min Temp		Precipitation		DPD		Wind speed		NO_x[b]	
		Mann-Kendall Results for Fog Predictor Variables											
	Deg	H	*p*	H	*p*	H	*p*	H	*p*	H	*p*	H	*p*
Redding	40°3′	—	—	0	1.2E-01	1	3.0E-02	—	—	—	—	—	—
Red Bluff	40°9′	1	1.8E-04	0	2.4E-01	0	1.0E-01	1	1.2E-02	1	4.8E-02	—	—
Chico[a]	39°5′	—	—	—	—	—	—	—	—	—	—	1	1.5E-05
Sacramento	38°3′	1	9.1E-06	0	4.4E-01	0	6.9E-01	1	7.0E-03	1	6.7E-07	1	7.1E-07
Stockton	37°5′	1	7.3E-05	0	6.3E-01	0	3.3E-01	1	3.9E-02	1	1.5E-04	—	—
Modesto	37°4′	—	—	—	—	—	—	—	—	—	—	1	2.4E-06
Fresno	36°5′	1	1.3E-06	0	8.3E-02	0	1.3E-01	1	3.0E-03	1	8.2E-07	1	3.2E-12
Visalia	36°2′	—	—	—	—	—	—	—	—	—	—	1	4.6E-07
Bakersfield	35°3′	1	6.0E-05	0	4.6E-01	0	2.6E-01	1	3.0E-03	1	4.3E-07	1	1.3E-08
		Sen Slopes and Percent Change for Fog Predictor Variables[c]											
	Deg	days/year	% Δ	°C/year	% Δ	mm/year	% Δ	°C/year	% Δ	$m \cdot s^{-1} \cdot year^{-1}$	% Δ	ppb/year	% Δ
Redding	40°3′	—	—	—	—	−8.4 ± 9.14	−36	—	—	—	—	—	—
Red Bluff	40°9′	−0.43 ± 0.21	−90	—	—	—	—	0.048 ± 0.045	33	−0.011 ± 0.010	−10	—	—
Chicoa	39°5′	—	—	—	—	—	—	—	—	—	—	−0.64 ± 0.22	−61
Sacramento	38°3′	−0.80 ± 0.23	−80	—	—	—	—	0.042 ± 0.029	42	−0.033 ± 0.010	−37	−1.2 ± 0.54	−58
Stockton	37°5′	−0.77 ± 0.33	−62	—	—	—	—	0.035 ± 0.034	35	−0.022 ± 0.013	−23	—	—
Modesto	37°4′	—	—	—	—	—	—	—	—	—	—	−1.0 ± 0.44	−50
Visalia	36°5′	—	—	—	—	—	—	—	—	—	—	−0.85 ± 0.28	−51
Fresno	36°2′	−0.87 ± 0.25	−70	—	—	—	—	0.049 ± 0.031	45	−0.024 ± 0.007	−33	−1.4 ± 0.23	−63
Bakersfield	35°3′	−0.61 ± 0.25	−76	—	—	—	—	0.064 ± 0.046	42	−0.027 ± 0.009	−33	−1.4 ± 0.32	−57

Note. H-test results of 1 demonstrate failure of the null hypothesis at 0.01 significance level. Results of H = 0 verify the null hypothesis, indicating no trend. Abbreviations: Min Temp = Minimum Temperature; DPD = Dew Point Depression; NO_x = Oxides of Nitrogen Concentration; PPB = Parts Per Billion; *p* = *p*-value.
[a]Record limited from 1980 to 2008. [b]Record limited from 1980 to 2014. [c]Only significant trends reported.

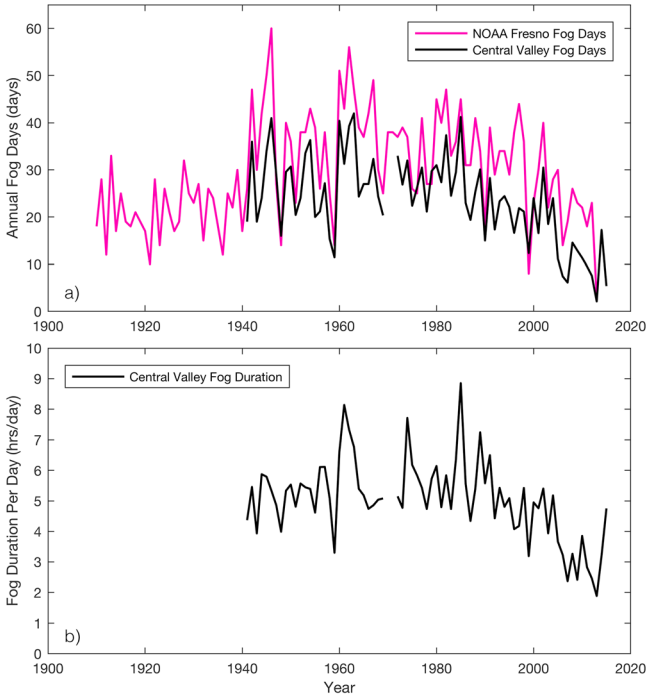

Figure 2. (a) NOAA record of fog days for Fresno (1909–2014) plotted with mean Central Valley fog days derived from hourly National Climatic Data Center records (1940–2016) and (b) average duration of fog episodes per fog day (1940–2016). NOAA = National Oceanic and Atmospheric Administration.

and regression statistics were calculated to compare their explanatory significance. Figures are included for all statistically significant findings.

4.2.1. Minimum Temperature

We focused on minimum temperature (T_{min}), because radiation fog most commonly forms after sunset (Figure S1) due to rapid surface radiative cooling. We would expect colder temperatures to be associated with frequent fog and low visibility, as it is easier for atmospheric moisture to reach saturation and condense. However, if the fog formation trend was heavily dependent on temperature, fog frequency would instead be the highest in the northern valley where it is colder on average, rather than the southern. When comparing the spatial gradient of fog days (Figure 3) and T_{min} (Figure S2a), temperature demonstrates significantly less N-S latitude consistency, with regions in the north, such as Redding and Red Bluff, occasionally reaching yearly-averaged T_{min} higher than locations hundreds of kilometers south, such as between 1950 and 1970, only to return to being the colder cities. However, more recent fog seasons—particularly in the last decade—show increased latitudinal consistency, with wintertime T_{min} throughout the valley both rising and becoming more homogenous.

With respect to historical trends, the valley experienced much less wintertime T_{min} warming than in other seasons. The T_{min} trend from 1980 to 2016 is not statistically significant (Figure S3a) and thus its direction cannot be determined (Table 1). A distinct warming signal is not evident until the last decade, suggesting that T_{min} did not influence the initial decline in fog days. These results then imply that T_{min} alone is not a dominate variable in fog frequency.

4.2.2. DPD

When the temperature is at or near the dew point, condensation of atmospheric moisture into fog droplets can occur, thus the variable DPD, calculated by subtracting dew point from ambient temperature, is expected to be related to fog formation. DPD must be near zero for fog droplet formation, so substantially foggy periods have low average DPD. A time series of DPD trends (Figure 4a) reveals that the northernmost sites Red Bluff and Redding have the highest

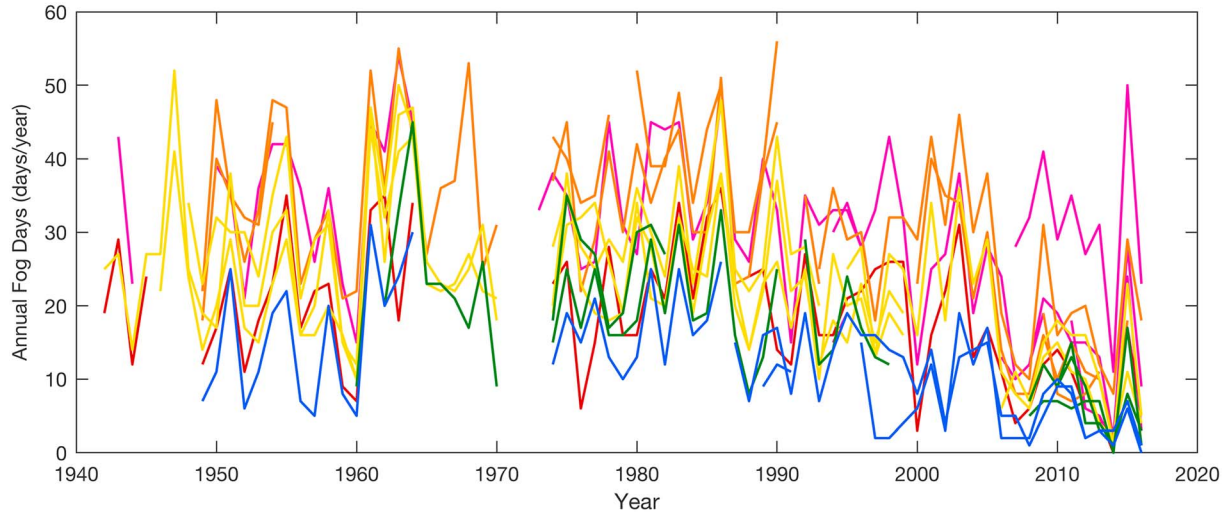

Figure 3. Plot of annual wintertime (November–March) fog days from 1940 to 2016 using National Climatic Data Center hourly meteorological database, with color gradient as defined in Figure 1. Rainbow color code represents latitude in 1° bins of sites from 35°N (red) to 40°N (blue). Dense fog defined as a day with visibility <400 m for any length of time. Years with <90% reporting are excluded.

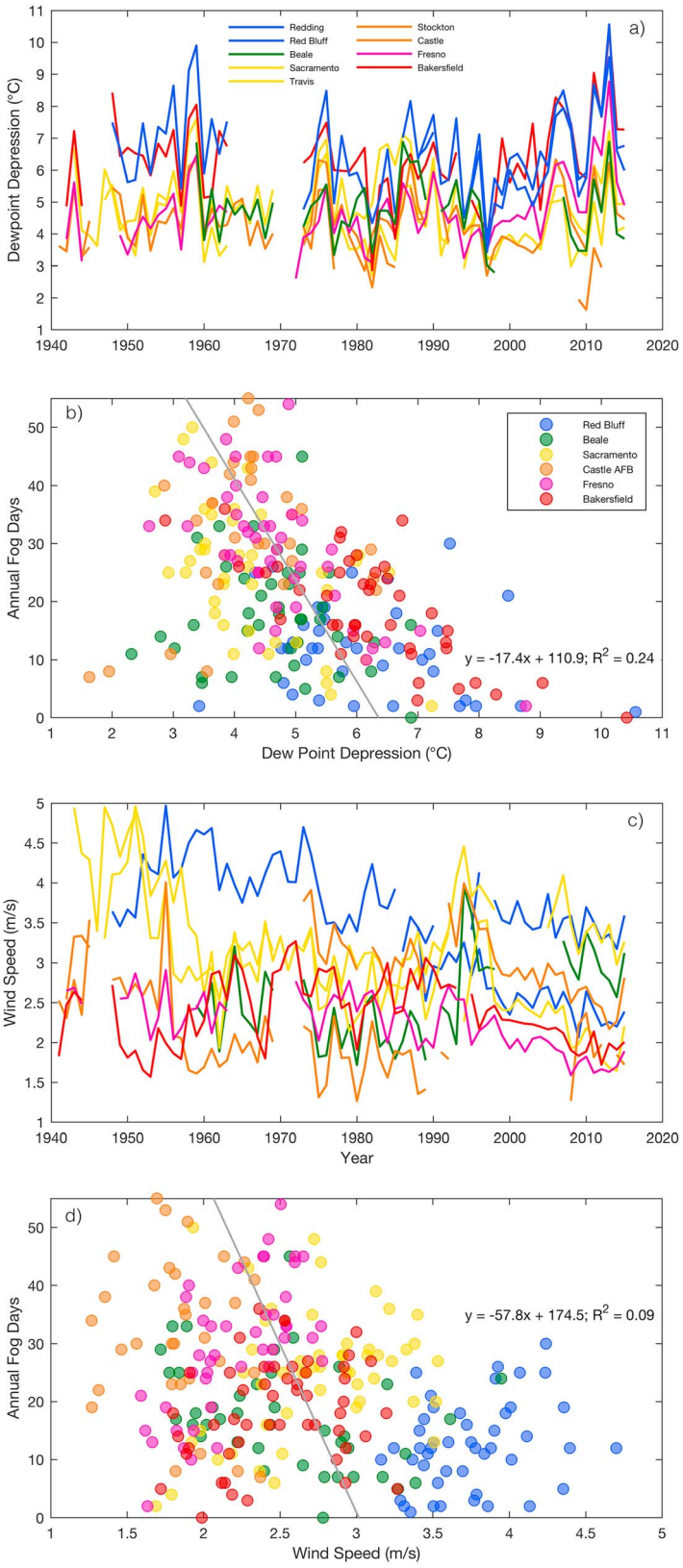

Figure 4. Time series of average (a) dew point depression and (c) wind speed for the annual fog season (November–March) from 1940 to 2016. Annual fog days plotted against (b) dew point depression and (d) wind speed. Rainbow color code represents latitude in 1° bins of sites from 35°N (red) to 40°N (blue).

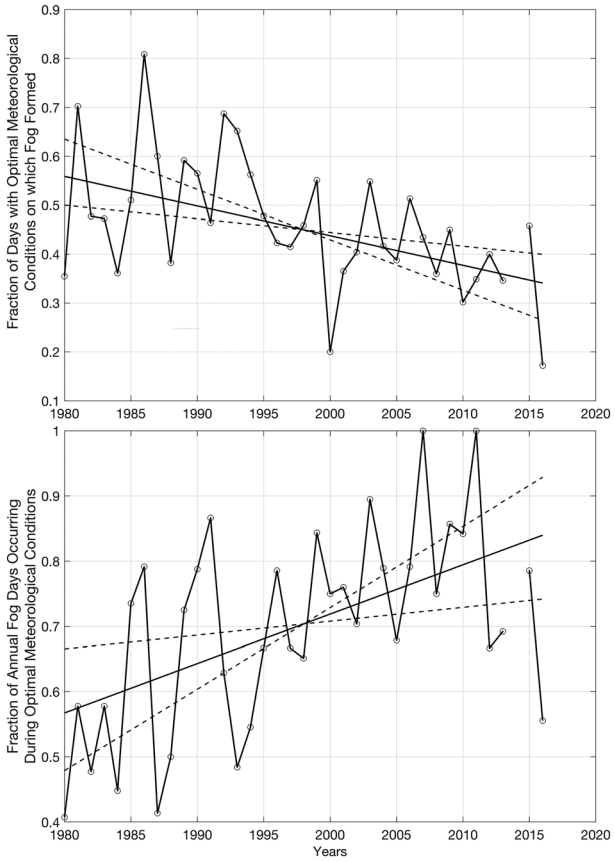

Figure 5. Historical trend for (a) the fraction of days with optimal meteorological conditions where fog actually occurs (sum of fog days during optimal conditions divided by number of days with optimal conditions) and (b) the fraction of total dense radiation fog days that occurred under optimal fog meteorological conditions (sum of fog days under optimal conditions divided by total number of fog days). Optimal meteorological conditions defined as dew point depression <4.2 °C and wind speed <2 m/s. Solid lines represents Sen slope fits, with dashed lines showing upper and lower confidence intervals. Year 2014 excluded because too few fog days occurred for robust statistics (< 5).

DPD, and thus largest average temperature decline needed during nighttime radiative cooling to reach condensation and fog formation. Meanwhile, Bakersfield, the most southern site, also has a relatively high seasonal DPD. This explains why its fog trend does not as consistently adhere to the north-south gradient of fog frequency (Figure 3)–the location is dryer than sites at proportional latitude, creating a larger threshold of DPD for fog formation. However, DPD alone cannot explain fog formation, because Bakersfield is one of the more frequently foggy sites. Thus, DPD can be an explanatory predictor, but clearly works in concert with other variables. This is further demonstrated by the lack of latitude consistency shown in Figure 4a, in which sites with the lowest DPD (shown in the yellow and green colors of Travis, Sacramento, and Beale) occur in central and northern locations of the valley that do not have the most fog.

Temporal trends of DPD reveal a valley-wide average increase of 39.5% from 1980 to 2016 ($p < 0.01$), suggesting that a decrease in fog days could be the result of concurrent changes in water availability and temperature (Table 1). However, when comparing Mann-Kendall trend test results for each decade from 1980 to 2016, results indicate that DPD began increasing at least 10 years after the decline in fog frequency; further, DPD decreased from 1990 to 2000, suggesting that it would enhance fog, but fog days continued declining. The high confidence intervals for the slope of DPD from 1980 to 2016 reflect the uncertainty in the strength and consistency of the trend (Table 1). Thus, while the overarching positive trend from 1980–2016 is statistically significant and likely impacting fog by inhibiting condensation, its initial increase does not agree with fog trends suggesting DPD alone is not responsible for the loss in fog days.

However, years of low DPD are well correlated with years of high fog frequency, with explanatory value for 24% of the annual variability (Figure 5b). This suggests that much can be understood about the stark interannual variability in fog events by looking at trends of water availability and temperature concurrently.

4.2.3. Precipitation

In contrast to temperature and DPD, precipitation displays a pronounced north-south gradient, with regions in the north consistently receiving more rain than those in the south (Figure S2b). While yearly precipitation exhibits strong interannual variability, the majority of the precipitation trend, aside from the droughts experienced from 2006 to 2010 and, most severely, 2012 to 2017, remains neutral with studies showing Northern and Central California getting wetter over the twentieth century and winter precipitation stable for the entire state (Killam et al., 2014). Only trends in Red Bluff were statistically significant ($p < 0.01$), demonstrating a 36.4% decline in precipitation, though with very wide confidence intervals (Table 1). The remaining sites exhibited no significant trend from 1980 to 2016.

Fog's sensitivity to precipitation remains an ongoing research question. While years of high rainfall are associated with an increase in fog events, many fog years are inversely correlated with precipitation totals (Figure S4). Additionally, we found that fog frequency has no correlation with the El Niño Southern Oscillation index, similar to the results of Herckes et al. (2015). The data suggest that there is some ideal precipitation amount for enhancing fog, and beyond that level fog is suppressed. This threshold likely exists because intense winter storms are associated with turbulent conditions unfavorable to fog formation. Similarly, frequent radiation fog can occur in years of low precipitation, because a significant rain event followed by high pressure and clear conditions is ideal for formation. Additionally, annual winter time precipitation demonstrates no statistically significant correlation with annual fog days, further highlighting the ambiguity (Figure S3b). Here we see that when holding a given annual precipitation constant, such as 300 mm, we might predictively expect a large range of potential fog days, from as low as 0 to as high as 50.

4.2.4. Wind Speed

Wind speed can play a significant role in radiation fog formation, as higher wind speeds increase surface mixing and inhibit radiative cooling after sunset; thus, we would spatially expect northern regions with less frequent fog to have higher wind speeds. However, average wind speed trends are inconsistent with spatial trends in fog frequency, lacking a clear gradient from north to south (Figure 4c).

Temporally, rather observing an increase in wind speed that would inhibit fog formation, a valley-wide ~27% decrease occurred ($p < 0.01$). While it correlates well with declining fog (Table 1), we would expect this to enhance fog formation through more stable atmospheric conditions and more rapid radiative cooling at night. This puzzling trend is consistent with recent evidence for a 5–15% midlatitude atmospheric stilling (Vautard et al., 2010), and suggests that had average wind speed not declined during this period, fog events would have been further diminished.

Wind speed demonstrated a low, but statistically significant predictive impact on fog frequency, explaining 9% of the variance (Figure 4d). Here we see that lower wind speeds are associated with higher fog frequency —a relationship likely made more complicated by trends in atmospheric stilling.

4.2.5. Segmenting Trends With Meteorologically Favorable Fog Conditions

We further investigated the fog trend by segmenting the meteorological record for conditions optimal for fog formation, defined as average daily DPD <4.2 °C and wind speed < 2m/s. The goal was to determine whether tule fog is more sensitive to the frequency of these meteorological conditions or some other potential driver when looking at daily data, rather than seasonal. The thresholds were determined by comparing the summary statistics for meteorology on foggy versus clear days. The frequency of optimal fog condition occurrence has no statistically significant trend during the period from 1980 to 2016, with a Mann-Kendall result of $H = 0$ at a 99% confidence interval (Figure S5). The frequency of favorable fog formation conditions remained consistent during this period despite increases in average DPD since 2000.

While there is no trend in the number of days with optimal fog conditions, the fraction of days where radiation fog actually occurred under these conditions declined significantly over this period ($p < 0.01$). In 1980, dense radiation fog occurred ~55% of the time when optimal fog conditions were met, but since 2010 fog only occurred ~35% of the time under these same conditions (Figure 5a). The observations suggest a mechanism unrelated to these meteorological variables is necessary to explain the observed decline in fog days.

This is further confirmed by analyzing the meteorology on the days when dense radiation fog forms (Figure 5b). The frequency of fog occurring under optimal conditions, relative to the total annual fog days, has increased significantly ($p < 0.01$), from ~50% (50% occurred outside optimal meteorological conditions) in the early 1980s, to ~80% since 2010 (20% occurred outside optimal meteorological conditions). This suggests that radiation fog formed much more frequently at higher DPDs and higher wind speeds in the 1980s than present day, which would be consistent with a reduction in the number of hygroscopic particles available for water to condense on. This effect is well documented in modeling studies which show that an increase in air pollutant concentration can allow for fog droplet growth under untraditional activation conditions where RH is below 100% (Charlson et al., 2001).

4.3. Air Pollution Trend

Central Valley population grew rapidly midcentury, with cities such as Fresno seeing a 103% growth from 1920 to 1950 and the Central Valley population growing by 52% from 1940 to 1950 alone (U.S. Census, 2011; Gregor, 1963), resulting in significant air pollution increases. Expansive oil extraction, rail freights, inefficient home heating, and increased vehicle use contributed to early pollution challenges, and agricultural burning and off-road equipment were unregulated.

While there are few observations of Central Valley NO_x prior to the mid-1960s, national EPA emission inventories for NO_x and PM_{10} give a picture of historical pollution trends (Figure 6), thus providing an estimate for increasing emissions and potential CCN availability midcentury. Nationally, derived PM_{10} emissions were greater than NO_x by mass prior to 1960 (Figure 6) but saw initial declines due to the effective mitigation of industrial sources (EPA, 2000). The magnitude of the national PM_{10} trend is consistent with California archival records from 1960 to 2005 for coefficient of haze, a retired measurement of particulate matter (Kirchstetter et al., 2017), though earlier PM_{10} inventory data are less reliable. Sulfur dioxide (SO_2)

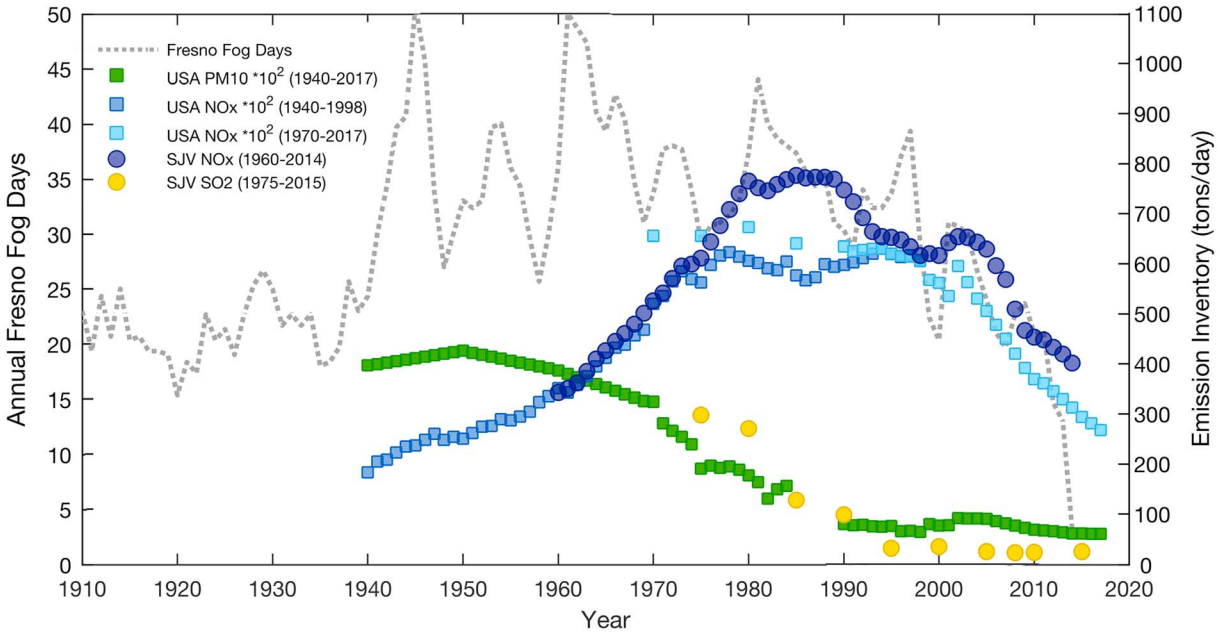

Figure 6. Time series of smoothed Fresno fog days from National Oceanic and Atmospheric Administration records (gray dotted line) plotted with national (square) and local (circle) emission inventories in tons per day. NO_x inventories represented by shades of blue points: two national NO_x inventories, ranging from 1940 to 1998 and 1970 to 2017, and one local San Joaquin Valley NO_x inventory from 1960 to 2014. National PM_{10} estimates from 1940 to 2017 represented by green squares. Local SO_2 estimates from 1975 to 2015 represented by yellow circles.

in the San Joaquin Valley was likely an important contributor to CCN midcentury, because the southern valley had considerable sulfate concentrations from local oil extraction (Jacob et al., 1987). However, due to its greater dominance as an air pollutant in much of the country, using a national inventory would not be representative of local trends in California where the use of coal for electricity generation is less prevalent. Local San Joaquin Valley SO_2 archives beginning in 1975 demonstrate that concentrations had already greatly increased by the 1970s and began rapidly falling decades prior to effective NO_x controls (Figure 6).

Instead, since the 1970s, NO_x has been the predominant inorganic pollutant—and most likely limiting wintertime CCN precursor—in the Central Valley. National NO_x emission inventories for 1940-1998 and 1970-2017 demonstrate the rise in NO_x sources with increasing fossil fuel use, followed by its subsequent decline beginning in the early 1980s, which is consistent with the locally developed fuel-based inventory for San Joaquin Valley. Implementation of California's vehicle tailpipe standards for hydrocarbons and carbon monoxide (1966), oxides of nitrogen (1971), and particulate matter from diesel-fueled vehicles (1982) began a substantial reduction in air pollution (California Air Resources Board, 2012). Most noteworthy was the implementation of the three-way catalytic converter on passenger vehicles in the early 1980s which began a stark trend of emission improvements, as seen in a 50% reduction in gasoline-NO_x emission from 1990 to 2010 in the San Joaquin Valley despite a 43% population growth (McDonald et al., 2012). Power plant emissions of NO_x also decreased from implementation of stack controls (Frost et al., 2006). Our SJV inventory suggests that in 1960, around half of the NO_x emissions are from stationary sources and the other half from mobile sources. By 2014, we estimate that mobile sources dominate (>80% of the NO_x total) in the San Joaquin Valley.

NH_4NO_3 concentration fell proportionally with measurements of NO_x, the limiting precursor, from 2000 to 2015, as Central Valley $PM_{2.5}$ declined at a rate of 2% a year (Pusede et al., 2016). This suggests that reductions in NO_x concentration directly reduced the availability of NH_4NO_3 as potential wintertime CCN. Trends in Fresno fog frequency and trends in San Joaquin Valley NO_x emissions have declined in concert (Figure 6), though fog frequency has significantly more variability. While the length of local records limits our

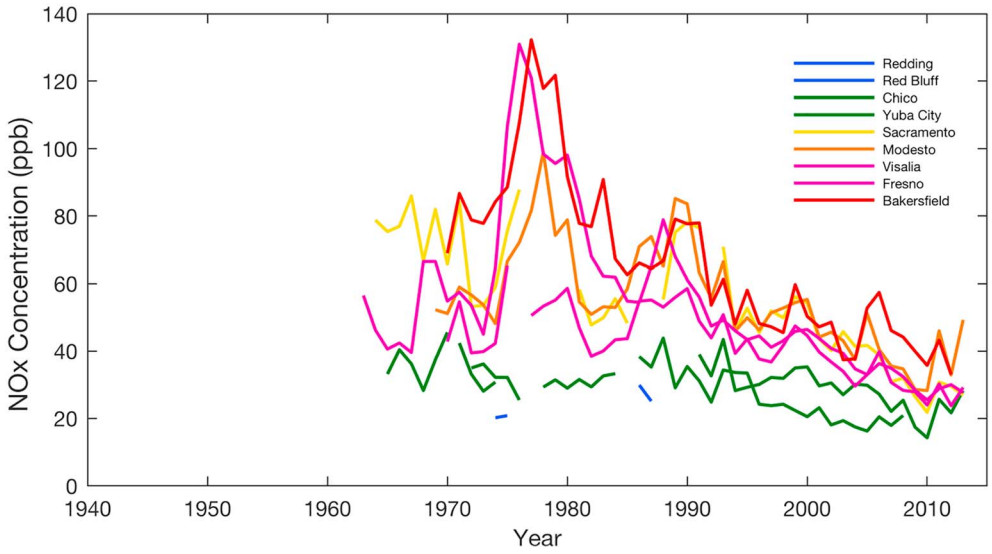

Figure 7. Time series of wintertime (November–March) NO_x concentration from 1962 to 2014 from the CARB archive. Color coding represents change in 1° of latitude, beginning at 40°N with cool colors representing northern cities and warm colors representing southern. ppb = parts per billion.

understanding of California pollutants prior to 1960s, we can infer from the slope of the local SO_2 (1975–2015) and national PM (1940–2017) inventories that other sources dominated and influenced the number of CCN available for fog formation.

These emission trends are confirmed by local wintertime NO_x concentration measurements for seven cities throughout the valley (Figure 7). The trend shows a rapid initial increase, followed by a ~50% decline from 1980 to 2014 ($p < 0.01$). Air pollution is the only fog contributor analyzed that began declining in the same decade as fog frequency and consistently continued declining from 1980 to 2016. Additionally, NO_x concentration exhibits a similar north-south gradient as seen with fog frequency, with concentration consistently highest in the south which is more populated and polluted (Figure 7). The north-south gradient remains persistent throughout the 50-year record despite the declining trend and interannual variability. Thus, NO_x decline has both a temporal and spatial signature consistent with that of fog frequency.

Annual fog days and NO_x concentration are significantly correlated ($p < 0.01$) with NO_x explaining an estimated 24% of the variance in fog frequency when examining all sites across all years (Figure 8a). This influence is further demonstrated when segmenting by the most impactful climate variable, DPD, in three quantiles by high, average, and low (Figure 8b). When DPD is high, representing high temperature and low water availability, fog frequency is less sensitive to additional CCN, explaining 29% of fog variance, because meteorological conditions are less sufficient for condensation. In this high DPD scenario, the regression slope is only 0.2, suggesting two additional fog days for every 10 parts per billion (ppb) increase of NO_x concentration. However, as DPD decreases and physical conditions get closer to causing condensation, the slope increases, representing fog frequency's increasing sensitivity to changes in air pollution. The coefficient of determination also increases, as NO_x has more explanatory significance. At low DPD conditions, with an average of 3.6 °C, NO_x concentration explains an estimated 46% of annual fog frequency. Thus, when average DPD is above 5 °C, sites are much less impacted by trends in NO_x, but given sufficiently low DPD, air pollution trends have a pronounced influence, with an estimated five additional fog days for every 10 ppb increase.

4.4. Separating Drivers of Short-Term and Long-Term Variability

Despite the strong influence of NO_x found in the fog frequency record, there remains considerable high frequency (short-term) variability in the record that is not observed in NO_x concentration. By decomposing the

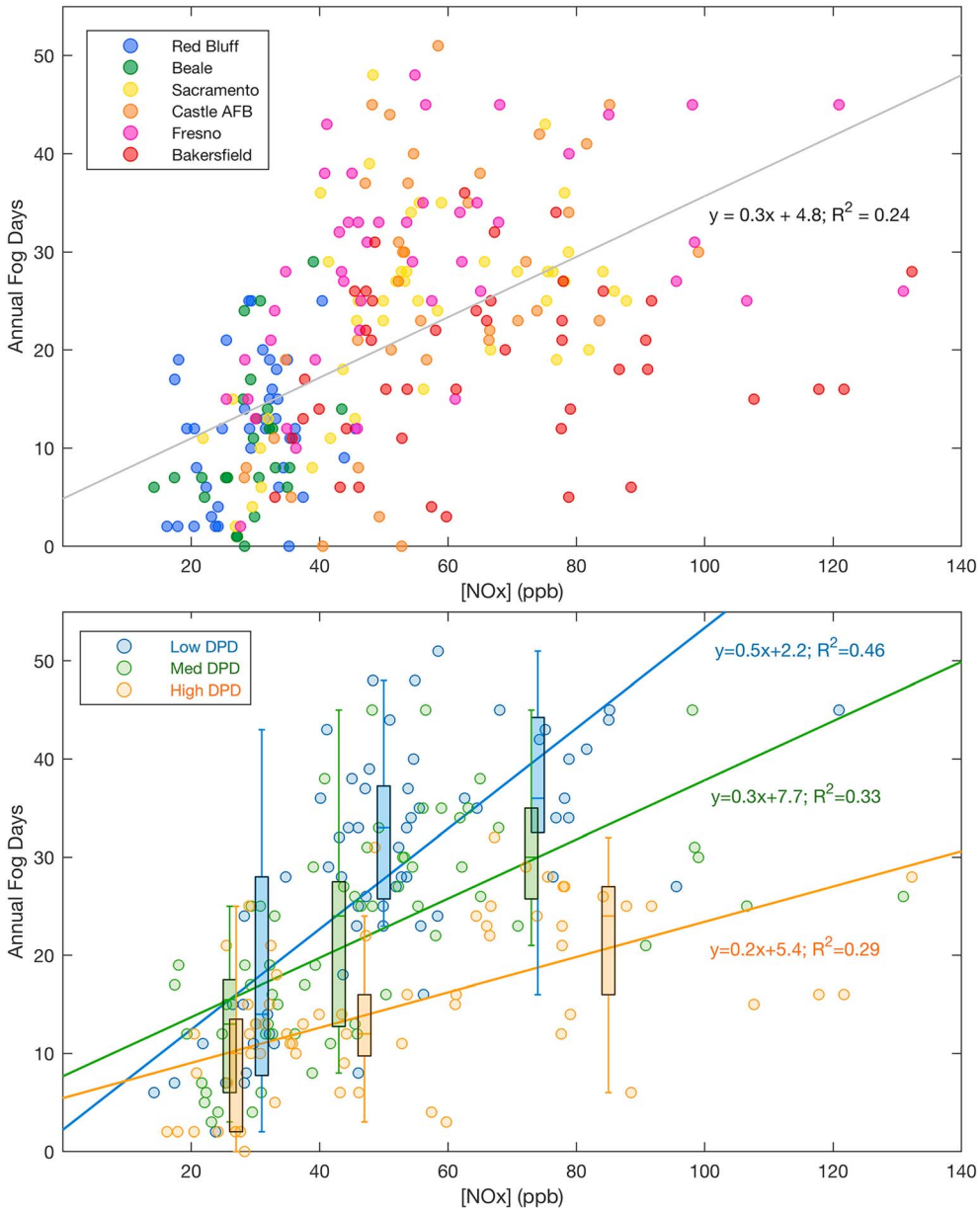

Figure 8. (a) Annual Fog Days plotted against NO_x concentration (ppb), with color coding representing 1° latitude and a fog day defined as any day where visibility < 400 m. (b) Correlation between fog days and NO_x segmented by three DPD quantiles, where blue represents the lowest quantile of DPD (1.6°–4.2°), green represents medium DPD (4.3°–5.6°), and orange represents high DPD (5.7°–9.0°). Fog day error bars demonstrated by the overlaid box plots for three quantiles of NO_x (low, medium, and high) per DPD bin. Total regression line displayed in both figures, where the coefficient of determination (R^2) is calculated by squaring Pearson's r to represent explanatory robustness of the predictor variable. DPD = dew point depression; ppb = parts per billion.

fog trends into high-frequency and low-frequency (long-term) components, we were able to quantify the impact meteorology is having on high frequency variability.

Analysis using a Lomb-Scargle periodogram identified the full 151 days included to represent each annual fog season ($p < 0.001$) as having the highest and most consistent spectral significance of any period in the data set, meaning that annual seasonal changes dominate the periodicity. The trend was therefore decomposed by applying a low pass filter with a period of 151 days on daily averages of fog season visibility, DPD, NO_x concentration, and wind speed for 1973–2014, the most complete time window for all variables. The high frequency data, determined as the residuals of the low pass filter, show that meteorology explains

Table 2
Separating High- and Low-Frequency Coefficients of Determination for Visibility Versus Dew Point Depression, Wind Speed, and NO_x

	Visibility
High-Frequency R^2	
DPD	0.29 (+)
[NOx]	0.10 (−)
Wind Speed	0.22 (+)
Low-Frequency R^2	
DPD	0.16 (+)
[NOx]	0.38 (−)
Wind Speed	0.11 (−)

Note. +/− indicates positive and negative correlations, respectively. DPD = dew point depression.

much more of the short-term variance than NO_x concentration. When testing the correlation of predictor variables with the daily visibility residuals and then calculating a coefficient of determination, DPD explains 29% and wind speed explains 22% of the variance in day-to-day average visibility (Table 2). By contrast, NO_x concentration captures only 10% of the variance. This indicates short-term variability in wintertime visibility is driven more by water availability, temperature, and wind speed than by processes associated with NO_x concentrations.

The low pass filter reveals long-term trends with the high frequency (short-term) variability removed. The trend component of each predictor variable was tested for correlation with the visibility trend, revealing that the NO_x concentration trend has the highest correlation with visibility, explaining 38% of the trend (Table 2), far more than the DPD, which explains 16%, or the wind speed, which explains 11%. The separation of long-term and short-term components clarifies that the NO_x trend better accounts for reductions in fog formation from 1980 to 2016, while meteorology better explains the short-term variability throughout the record.

5. Summary and Conclusions

The short-term variability in meteorology correlates with the strong variability of fog events, but cannot explain the observed longer-term trends in fog frequency. DPD has the strongest explanatory robustness of the meteorological variables, as potential to form fog is clearly a function of both water availability and sufficiently low temperature. Additionally, until recently, low wind speed had a strong correlation with years of frequent fog events. The recent "atmospheric stilling" observed in the wind speed record favors fog frequency, thus masking the even more complete collapse of the fog season that would have likely occurred otherwise.

The coherence of both the spatial (north-south) gradient and historical (upward-then-downward) trend is unique to fog frequency and air pollution. Despite some changes to climate in recent decades, the frequency of optimal fog conditions remains stable, yet fog continues to decline relative to the number of low DPD and low wind speed days occurring each year. Additionally, nearly all tule fog events in recent years occur during the most favorable fog conditions, whereas 35 years ago fog occurred on warmer days with higher wind speeds and less water availability much more frequently. This is consistent with the impact of higher air pollution historically causing a higher number concentration of hygroscopic particles for condensation, as well as pollution causing nontraditional activation of droplets when RH < 100%.

Controlling for the large interannual variability in DPD further elucidates the statistically robust relationship between fog frequency and air pollution, particularly under conditions of low DPD. When annual average conditions have sufficient atmospheric moisture and low temperatures necessary to support condensation, fog frequency is significantly more sensitive to the resulting increases in condensation nuclei from high pollution concentrations. This relationship is the weakest in fog seasons where DPD is high, but it is still significant. Our findings demonstrate that in low DPD conditions, a decrease of five fog days per year occurred for every 10 ppb NO_x decrease over the past 36 years. The upward trend in fog frequency from 1930 to 1970 was likely driven by increases in emissions of other air pollutants including primary particles and possibly SO_2, but no observational data are available to further constrain the specific pollutants involved prior to the initiation of the long-term air pollution measurement network in California.

Changes in fog frequency have broad impacts on transportation safety, agricultural production, drought resilience, and climate. While the interannual influence of meteorology is key to understanding its year-to-year signal, our analysis demonstrates that changes in air pollution emissions are the main driver of the observed long-term trend of radiation fog frequency, and that reducing air pollution has had the added benefit of reducing tule fog in California's Central Valley. The impacts of reductions in air pollution emissions on fog frequency, and resulting changes for the agricultural economy, transportation safety, and climate, should be analyzed in future assessments of the cobenefits of air pollution controls.

Acknowledgments

This material is based upon work supported by the National Science Foundation Graduate Research Fellowship (grants 1106400 and 1752814). Any conclusions expressed in this material are those of the authors and do not necessarily reflect the views of the National Science Foundation. The authors gratefully acknowledge California Agricultural Experiment Station and USDA McIntire-Stennis Cooperative Forestry Program, as well as funding from the National Research Council of Italy. Derived averages for the explanatory variables investigated are found online (https://figshare.com/articles/Central_Valley_Wintertime_Climate_Averages/7859978). We appreciate the helpful suggestions from the three anonymous reviewers whose feedback greatly improved the manuscript.

References

American Lung Association (2016). *State of the air 2016*, (Vol. 56). Chicago, IL: American Lung Association. https://doi.org/10.1017/CBO9781107415324.004

Andreae, M. O., & Rosenfeld, D. (2008). Aerosol-cloud-precipitation interactions. Part 1. The nature and sources of cloud-active aerosols. *Earth-Science Reviews*, *89*(1–2), 13–41. https://doi.org/10.1016/j.earscirev.2008.03.001

Ashley, W. S., Strader, S., Dziubla, D. C., & Haberlie, A. (2015). Driving blind: Weather-related vision hazards and fatal motor vehicle crashes. *Bulletin of the American Meteorological Society*, *96*(May), 755–778. https://doi.org/10.1175/BAMS-D-14-00026.1

Baldocchi, D., & Waller, E. (2014). Winter fog is decreasing in the fruit growing region of the Central Valley of California. *Geophysical Research Letters*, *41*, 799–804. https://doi.org/10.1002/2014GL060018

Baldocchi, D., & Wong, S. (2008). Accumulated winter chill is decreasing in the fruit growing regions of California. *Climatic Change*, *87*, 153–166. https://doi.org/10.1007/s10584-007-9367-8

Battye, W., Aneja, V. P., & Roelle, P. A. (2003). Evaluation and improvement of ammonia emissions inventories. *Atmospheric Environment*, *37*(27), 3873–3883. https://doi.org/10.1016/S1352-2310(03)00343-1

Bergot, T., & Guedalia, D. (1994). Numerical forecasting of radiation fog. Part I: Numerical model and sensitivity tests. *Monthly Weather Review*, *122*(6), 1218–1230. https://doi.org/10.1175/1520-0493(1994)122<1218:NFORFP>2.0.CO;2

Bianco, L., Djalalova, I. V., King, C. W., & Wilczak, J. M. (2011). Diurnal evolution and annual variability of boundary-layer height and its correlation to other meteorological variables in California's Central Valley. *Boundary-Layer Meteorology*, *140*(3), 491–511. https://doi.org/10.1007/s10546-011-9622-4

Brimblecombe, P. (1977). London air pollution, 1500–1900. *Atmospheric Environment*, *11*(12), 1157–1162. https://doi.org/10.1016/0004-6981(77)90091-9

Burkey, J. (2006). *A non-parametric monotonic trend test computing Mann-Kendall Tau, Tau-b, and Sens Slope written in Mathworks-MATLAB implemented using matrix rotations*. Seattle, Washington. USA: King County, Department of Natural Resources and Parks, Science and Technical Services Section. http://www.mathworks.com/matlabcentral/fileexchange/authors/23983

California Air Resources Board (2009). *CEPAM: 2009 Almanac—Standard emissions tool*. Sacramento, CA: California Air Resources Board. https://www.arb.ca.gov/app/emsinv/fcemssumcat2009.php

California Air Resources Board (2012). Key events in the history of air quality in California. Retrieved from http://www.retailcrc.org/RegGuidance/Lists/RNGList/Attachments/659016/GCA00046.pdf

California Department of Food and Agriculture. (2018). *California County Agricultural Commissioners' Reports: Crop Year 2016-2017*. Sacramento, CA. Retrieved from https://www.nass.usda.gov/Statistics_by_State/California/Publications/AgComm/2014/2014cropyearcactb00.pdf

Charlson, R. J., Seinfeld, J. H., Nenes, A., Kulmala, M., Laaksonen, A., & Facchini, M. C. (2001). Reshaping the theory of cloud formation. *Science*, *292*(5524), 2025–2026. https://doi.org/10.1126/science.1060096

Chow, J. C., Chen, L.-W. A., Watson, J. G., Lowenthal, D. H., Magliano, K. A., Turkiewicz, K., & Lehrman, D. E. (2006). PM2.5 chemical composition and spatiotemporal variability during the California Regional PM10/PM2.5 Air Quality Study (CRPAQS). *Journal of Geophysical Research*, *111*, D10S04. https://doi.org/10.1029/2005JD006457

Energy Information Administration (2017). *State energy data system (SEDS): 1960–2016*. Washington, DC: Energy Information Administration, U.S. Department of Energy. https://www.eia.gov/state/seds/

Environmental Protection Agency (2000). *National air pollutant emission trends, 1900–1998*. Durham, North Carolina: Environmental Protection Agency.

Fischer, D. T., Still, C. J., & Williams, A. P. (2009). Significance of summer fog and overcast for drought stress and ecological functioning of coastal California endemic plant species. *Journal of Biogeography*, *36*(4), 783–799. https://doi.org/10.1111/j.1365-2699.2008.02025.x

Frost, G. J., McKeen, S. A., Trainer, M., Ryerson, T. B., Neuman, J. A., Roberts, J. M., et al. (2006). Effects of changing power plant NO_x emissions on ozone in the eastern United States: Proof of concept. *Journal of Geophysical Research*, *111*, D12306. https://doi.org/10.1029/2005JD006354

Gilardoni, S., Massoli, P., Giulianelli, L., Rinaldi, M., Paglione, M., Pollini, F., et al. (2014). Fog scavenging of organic and inorganic aerosol in the Po valley. *Atmospheric Chemistry and Physics*, *14*(13), 6967–6981. https://doi.org/10.5194/acp-14-6967-2014

Gregor, H. (1963). Spatial disharmonies in California population growth. *Geographical Review*, *53*(1), 100–122. https://doi.org/10.2307/212811

Gultepe, I., Tardif, R., Michaelides, S. C., Cermak, J., Bott, A., Bendix, J., et al. (2007). Fog research: A review of past achievements and future perspectives. *Pure and Applied Geophysics*, *164*(6–7), 1121–1159. https://doi.org/10.1007/s00024-007-0211-x

Hassler, B., McDonald, B. C., Frost, G. J., Borbon, A., Carslaw, D. C., Civerolo, K., et al. (2016). Analysis of long-term observations of NOx and CO in megacities and application to constraining emissions inventories. *Geophysical Research Letters*, *43*, 9920–9930. https://doi.org/10.1002/2016GL069894

Herckes, P., Marcotte, A. R., Wang, Y., & Collett, J. L. (2015). Fog composition in the Central Valley of California over three decades. *Atmospheric Research*, *151*, 20–30. https://doi.org/10.1016/j.atmosres.2014.01.025

Jacob, D. J., Shair, F. H., Waldman, J. M., Munger, J. W., & Hoffman, M. (1986). Transport and oxidation of SO2 in a stagnant foggy valley. *Atmospheric Environment*, *21*(6), 1305–1314. https://doi.org/10.1016/0004-6981(67)90077-7

Jacob, D. J., Shair, F. H., Waldman, J. M., Munger, J. W., & Hoffman, M. (1987). Transport and Oxidation of SO2 in a Stagnant Foggy Valley. *Atmospheric Environment*, *21*(6), 1305–1314. https://doi.org/10.1016/0004-6981(67)90077-7

Kendall, M. G. (1955). *Rank correlation methods*, (2nd ed.). Oxford, England: Hafner Publishing Co.

Killam, D., Bui, A., LaDochy, S., Ramirez, P., Willis, J., & Patzert, W. (2014). California getting wetter to the north, drier to the south: Natural variability or climate change? *Climate*, *2*(3), 168–180. https://doi.org/10.3390/cli2030168

Kirchstetter, T. W., Preble, C. V., Hadley, O. L., Bond, T. C., & Apte, J. S. (2017). Large reductions in urban black carbon concentrations in the United States between 1965 and 2000. *Atmospheric Environment*, *151*, 17–23. https://doi.org/10.1016/j.atmosenv.2016.11.001

Klemm, O., & Lin, N. H. (2016). What causes observed fog trends: Air quality or climate change? *Aerosol and Air Quality Research*, *16*(5), 1131–1142. https://doi.org/10.4209/aaqr.2015.05.0353

Kokkola, H., Romakkaniemi, S., & Laaksonen, A. (2002). On the formation of radiation fogs under heavily polluted conditions. *Atmospheric Chemistry and Physics Discussions*, *3*(1), 389–411. http://doi.org/10.5194/acpd-3-389-2003

Kulmala, M., Korhonen, P., Laaksonen, A., & Vesala, T. (1995). Changes in cloud properties due to NOx emissions. *Geophysical Research Letters*, *22*(3), 239–242. https://doi.org/10.1029/94GL02691

Kulmala, M., Laaksonen, A., Charlson, R. J., & Korhonen, P. (1997). Clouds without supersaturation. *Nature*, *388*(6640), 336–337. https://doi.org/10.1038/41000

Kulmala, M., Toivonen, A., Mattila, T., & Korhonen, P. (1998). Variations of cloud droplet concentrations and the optical properties of clouds due to changing hygroscopicity: A model study. *Journal of Geophysical Research*, *103*(D13), 16183–16195. https://doi.org/10.1029/98JD00880

Laaksonen, A., Korhonen, P., Kulmala, M., & Charlson, R. J. (1998). Modification of the Köhler equation to include soluble trace gases and slightly soluble substances. *Journal of the Atmospheric Sciences*, *55*(5), 853–862. https://doi.org/10.1175/1520-0469(1998)055<0853:MOTKHE>2.0.CO;2

Lee, T. F. (1987). Urban clear islands in California central valley fog. *Monthly Weather Review*, *115*(8), 1794–1796. https://doi.org/10.1175/1520-0493(1987)115<1794:UCIICC>2.0.CO;2

Lomb, N. R. (1976). Least-squares frequency analysis of unequally spaced data. *Astrophysics and Space Science.*, *39*, 447–462. https://doi.org/10.1007/BF00648343

Luedeling, E., Zhang, M., Luedeling, V., & Girvetz, E. H. (2009). Sensitivity of winter chill models for fruit and nut trees to climatic changes expected in California's Central Valley. *Agriculture, Ecosystems and Environment*, *133*(1–2), 23–31. https://doi.org/10.1016/j.agee.2009.04.016

Mann, H. (1945). Nonparametric Tests Against Trend. *Econometrica*, *13*(3), 245–259. https://doi.org/10.2307/1907187

McDonald, B. C., Dallmann, T. R., Martin, E. W., & Harley, R. A. (2012). Long-term trends in nitrogen oxide emissions from motor vehicles at national, state, and air basin scales. *Journal of Geophysical Research*, *117*, D00V18. https://doi.org/10.1029/2012JD018304

Petters, M. D., & Kreidenweis, S. M. (2007). A single parameter representation of hygroscopic growth and cloud condensation nucleus activity-Part 3: Including surfactant partitioning. *Atmospheric Chemistry and Physics*, *13*(2), 1081–1091. https://doi.org/10.5194/acp-13-1081-2013

Pusede, S. E., & Cohen, R. C. (2012). On the observed response of ozone to NOx and VOC reactivity reductions in San Joaquin Valley California 1995-present. *Atmospheric Chemistry and Physics*, *12*, 8323–8339. https://doi.org/10.5194/acp-12-8323-2012

Pusede, S. E., Duffey, K. C., Shusterman, A. A., Saleh, A., Laughner, J. L., Wooldridge, P. J., et al. (2016). On the effectiveness of nitrogen oxide reductions as a control over ammonium nitrate aerosol. *Atmospheric Chemistry and Physics*, *16*(4), 2575–2596. https://doi.org/10.5194/acp-16-2575-2016

Roach, W. T., Brown, R., Caughey, S. J., Garland, J. A., & Readings, C. J. (1976). The physics of radiation fog: I—A field study. *Quarterly Journal of the Royal Meteorological Society*, *102*(432), 313–333. https://doi.org/10.1002/qj.49710243204

Russell, A. R., Valin, L. C., & Cohen, R. C. (2012). Trends in OMI NO_2 observations over the United States: Effects of emission control technology and the economic recession. *Atmospheric Chemistry and Physics*, *12*(24), 12197–12209. https://doi.org/10.5194/acp-12-12197-2012

Salas, W., Green, P., Frolking, S., Li, C., & Boles, S. (2006). *Estimating irrigation water use for California agriculture: 1950s to present*. Sacramento: California Energy Commission. Retrieved from. http://www.energy.ca.gov/2006publications/CEC-500-2006-057/CEC-500-2006-057.PDF

Scargle, J. D. (1982). Studies in astronomical time series analysis. II. Statistical Aspects of Spectral Analysis of Unevenly Spaced Data. *Astrophysical Journal*, *263*, 835–853. https://doi.org/10.1086/160554

Schiferl, L. D., Heald, C. L., Nowak, J. B., Holloway, J. S., Neuman, J. A., Bahreini, R., et al. (2014). An investigation of ammonia and inorganic particulate matter in California during the CalNex campaign. *Journal of Geophysical Research: Atmospheres*, *119*, 1883–1902. https://doi.org/10.1002/2013JD020765

Sen, P. K. (1968). Robustness of some nonparametric procedures in linear models. *The Annals of Mathematical Statistics*, *39*(6), 1913–1922. https://doi.org/10.1214/aoms/1177698021

Senn, C. L. (1948). General atmospheric pollution: Los Angeles "smog". *American Journal of Public Health Nation's Health*, *38*, 962–965. https://doi.org/10.2105/AJPH.38.7.962

Suckling, P. W., & Mitchell, M. D. (1988). Fog climatology of the Sacramento urban area. *The Professional Geographer*, *40*(2), 186–194. https://doi.org/10.1111/j.0033-0124.1988.00186.x

Theil, H. (1950). A rank-invariant method of linear and polynomial regression analysis I. *Nederlandse Akademie Wetenchappen*, *23*(Series A), 386–392. https://doi.org/10.1007/978-94-011-2546-8

U.S. Census Bureau (2011). Historical US census populations of places, towns, and cities in California 1850-2010. Retrieved from http://www.dof.ca.gov/Reports/Demographic.../2010-1850_STCO_IncCities-FINAL.xls

Underwood, S. J., Ellrod, G. P., & Kuhnert, A. L. (2004). A multiple-case analysis of nocturnal radiation-fog development in the Central Valley of California utilizing the GOES nighttime fog product. *Journal of Applied Meteorology*, *43*(2), 297–311. https://doi.org/10.1175/1520-0450(2004)043<0297:AMAONR>2.0.CO;2

Underwood, S. J., & Hansen, C. (2008). Investigating urban clear islands in fog and low stratus clouds in the San Joaquin Valley of California. *Physical Geography*, *29*(5), 442–454. https://doi.org/10.2747/0272-3646.29.5.442

Vautard, R., Cattiaux, J., Yiou, P., Thépaut, J.-N., & Ciais, P. (2010). Northern Hemisphere atmospheric stilling partly attributed to an increase in surface roughness. *Nature Geoscience*, *3*(11), 756–761. https://doi.org/10.1038/ngeo979

Wilkins, E. T. (1954). Air pollution aspects of the London fog of December 1952. *Quarterly Journal of the Royal Meteorological Society*, *80*(344), 267–271. https://doi.org/10.1002/qj.49708034420

Williams, A. P., Gentine, P., Moritz, M. A., Roberts, D. A., & Abatzoglou, J. T. (2018). Effect of reduced summer cloud shading on evaporative demand and wildfire in coastal Southern California. *Geophysical Research Letters*, *45*, 5653–5662. https://doi.org/10.1029/2018GL077319